AIP | Chaos
An Interdisciplinary Journal of Nonlinear Science
25TH ANNIVERSARY

Synchronization, non-linear dynamics and low-frequency fluctuations: Analogy between spontaneous brain activity and networked single-transistor chaotic oscillators

Ludovico Minati, Pietro Chiesa, Davide Tabarelli, Ludovico D'Incerti, and Jorge Jovicich

Citation: Chaos: An Interdisciplinary Journal of Nonlinear Science **25**, 033107 (2015); doi: 10.1063/1.4914938
View online: http://dx.doi.org/10.1063/1.4914938
View Table of Contents: http://scitation.aip.org/content/aip/journal/chaos/25/3?ver=pdfcov
Published by the AIP Publishing

CHAOS **25**, 033107 (2015)

Synchronization, non-linear dynamics and low-frequency fluctuations: Analogy between spontaneous brain activity and networked single-transistor chaotic oscillators

Ludovico Minati,[1,2,a)] Pietro Chiesa,[2] Davide Tabarelli,[2] Ludovico D'Incerti,[3] and Jorge Jovicich[2]
[1]*Scientific Department, Fondazione IRCCS Istituto Neurologico Carlo Besta, Milan, Italy*
[2]*Center for Mind/Brain Sciences, University of Trento, Trento, Italy*
[3]*Neuroradiology Unit, Fondazione IRCCS Istituto Neurologico Carlo Besta, Milan, Italy*

(Received 17 November 2014; accepted 2 March 2015; published online 17 March 2015)

In this paper, the topographical relationship between functional connectivity (intended as inter-regional synchronization), spectral and non-linear dynamical properties across cortical areas of the healthy human brain is considered. Based upon functional MRI acquisitions of spontaneous activity during wakeful idleness, node degree maps are determined by thresholding the temporal correlation coefficient among all voxel pairs. In addition, for individual voxel time-series, the relative amplitude of low-frequency fluctuations and the correlation dimension (D_2), determined with respect to Fourier amplitude and value distribution matched surrogate data, are measured. Across cortical areas, high node degree is associated with a shift towards lower frequency activity and, compared to surrogate data, clearer saturation to a lower correlation dimension, suggesting presence of non-linear structure. An attempt to recapitulate this relationship in a network of single-transistor oscillators is made, based on a diffusive ring ($n = 90$) with added long-distance links defining four extended hub regions. Similarly to the brain data, it is found that oscillators in the hub regions generate signals with larger low-frequency cycle amplitude fluctuations and clearer saturation to a lower correlation dimension compared to surrogates. The effect emerges more markedly close to criticality. The homology observed between the two systems despite profound differences in scale, coupling mechanism and dynamics appears noteworthy. These experimental results motivate further investigation into the heterogeneity of cortical non-linear dynamics in relation to connectivity and underline the ability for small networks of single-transistor oscillators to recreate collective phenomena arising in much more complex biological systems, potentially representing a future platform for modelling disease-related changes. © *2015 AIP Publishing LLC*. [http://dx.doi.org/10.1063/1.4914938]

Understanding brain function requires considering two properties that are increasingly deemed fundamental: (1) structural connections among cortical regions and, consequently, activity synchronization are architected so that a minority of areas have a disproportionately high number of connections, including long-distance connections, conferring them the role of "hubs"; (2) brain circuits are somehow attuned so that their collective operation takes place preferentially close to the "point of criticality", that is, fluctuating around order-to-chaos transition, which may confer specific computational advantages. Previous studies have shown that these properties can be inferred from time-series acquired using functional MRI during idle wakefulness, representing intrinsic or "spontaneous" brain activity. However, not much is known regarding whether the known differences in connectivity among cortical regions are topographically associated with generation of activity having diverse non-linear dynamical properties, particular with regards to hallmarks of possible chaoticity. Here, we addressed this question and found that the cortical areas that are more intensely synchronized with other regions tend to generate activity with stronger low-frequency fluctuations and more evident non-linear structure than the others. We speculated that this could indicate a shift of the underlying neural activity towards chaos and went on to test this hypothesis indirectly by studying a simple network of electronic oscillators, in which, despite profound structural and dynamical differences, a similar relationship was observed.

I. INTRODUCTION

The brain is a complex non-linear system characterized by non-trivial topological and dynamical properties. Its structural connectivity exhibits small-world and scale-free organization that hinges around "cortical hub" regions. These regions, including precuneus, superior-lateral parietal, and medial frontal cortex, are heavily interconnected and hypothesized to subserve high-order cognitive processes.[1–4] Further, the brain plausibly operate collectively as a thermodynamic system close to a phase transition corresponding to

---

[a)] Author to whom correspondence should be addressed. Electronic addresses: lminati@ieee.org, ludovico.minati@unitn.it, and lminati@istituto-besta.it. Tel.: +39 335 486670. Present address: Centre for Mind/Brain Sciences, University of Trento, via delle Regole 101, 38123 Mattarello TN, Italy.

instability between laminar and chaotic flow. As such, it can rapidly explore different dynamical regimes, generating avalanches of activity that propagate across the entire network.[5–7]

Based on realistic models of structural connectivity, numerical simulations predict the emergence of functional connectivity (activity synchronization between regions) in the form of discrete "resting-state" networks (RSNs), such as the "default-mode network" and "fronto-parietal network."[7–10] These networks have been detected by means of independent component analysis of blood oxygen level dependent (BOLD) time-series recorded using functional MRI during awake idleness (resting-state), whose fluctuations primarily represent spontaneous neural activity.[11,12] Graph-based analyses of BOLD signal synchronization have also confirmed high node degree of functional connectivity (representing a measure of "synchronization density") in the aforementioned cortical hub regions, in broad agreement with the underlying structural connectivity.[13–16]

The temporal resolution of BOLD recordings is constrained to the order of seconds by the underlying neurovascular response and measurements are contaminated by non-neural physiological noise, which is often subject to aliasing due to limited sampling rate.[17,18] Despite these severe limitations, the temporal variance of BOLD time-series is sufficiently representative for reliable identification of the RSNs, possibly as a consequence of scale-free activity with $1/f^{\beta}$-like power spectrum, and as such plausibly contains information also about non-linear dynamics of the underlying neural activity.[17,19]

A current question is whether there are observable non-linear dynamical and spectral properties of BOLD fluctuations which reflect the local influence of connectivity on temporal dynamics. Understanding the topographical relationship between brain connectivity and regional non-linear dynamics is relevant both theoretically and for the development of neuropsychiatric disease biomarkers, and, despite the above limitations, functional MRI may be well-suited for addressing this issue in virtue of its high spatial resolution.[20]

Point-process modelling of BOLD time-series has been remarkably successful in providing a compact representation of RSN emergence and enabling explicit demonstration of collectively critical oscillation.[21,22] Evidence that the brain operates close to phase transition to chaos confers relevance to well-established univariate measures of dynamical non-linearity, such as the correlation dimension (D_2) and the largest Lyapunov exponent, which to date have been infrequently applied to functional MRI time-series.[23,24] Characterization of spectral features is also important given that phase transitions are generally associated with profound changes in the spectral moments of oscillatory variables.[25–27] Recent increases in the sampling rate of functional MRI have made it possible to study inter-regional spectral differences, often represented with power-law frequency scaling coefficients or relative Fourier amplitudes of low frequencies (typically <0.1 Hz).[19,28,29]

At the same time, the fact that realistic RSNs emerge even in highly simplified simulation scenarios, for example, from networked phase (Kuramoto) oscillators or discrete excitable units, raises the intriguing possibility of recapitulating some dynamical phenomena underlying brain function in other physical systems, where direct manipulation of connectivity is possible and causal relationships between connectivity and non-linear dynamics can be explored experimentally.[8–10,30]

In particular, it has recently been shown that single-transistor oscillators can exhibit strikingly complex activity depending on an easily tunable control parameter (DC voltage source series resistance), oscillating periodically, chaotically, or close to criticality.[31] An experimental investigation of a ring of 30 diffusively coupled such oscillators, each consisting of a bipolar junction transistor, three reactive components and a resistor, has furthermore demonstrated the spontaneous formation of multi-scale community structure as a function of coupling strength, with elements of similarity to the modular organization observed in brain networks.[32] While that study was conducted for an elementary structural connectivity scenario (a ring), it is possible to construct arbitrarily complex networks. Coupled single-transistor oscillators therefore represent an undemanding experimental platform with which one may attempt to recapture associations between brain connectivity and non-linear dynamics observed through BOLD time-series either empirically or in numerical simulation.

In this study, the topographical correspondence between functional connectivity (node degree), spectral and non-linear dynamical features (relative amplitude of low-frequency fluctuations, correlation dimension D_2 and its saturation δD_2 across embedding dimensions) across cortical regions of the healthy human brain was empirically assessed. A highly simplified model of brain connectivity was also implemented in the form of single-transistor oscillators arranged as a ring with superimposed long-distance links creating four extended hubs. The relationship between connectivity and non-linear dynamics in this network was evaluated for different dynamical regimes (close to criticality, chaotic) and compared to results from brain data.

II. FUNCTIONAL MRI METHODS

A. Data acquisition

Brain data from 10 young unrelated healthy participants were downloaded from the repository of the Human Connectome Project.[33] The participants were scanned at Washington University on a 32-channel 3.0 T unit (Skyra Connectome, Siemens AG, Erlangen, Germany), following provision of written informed consent and in accordance to study procedures approved by the institutional review board (Ref. 201204036).

For each participant, 1200 resting-state functional volumes sensitized to the BOLD contrast were acquired twice, with RL and LR phase encoding direction, using a gradient-echo echo-planar sequence having multiband factor $=8$, TR $=720$ ms (corresponding to sample rate ~ 1.4 Hz), TE of $=33.1$ ms, flip angle $=52°$, 104×90 matrix size, 72 slices, 2 mm isotropic voxel size, bandwidth $=2290$ Hz/pixel, echo spacing $=0.58$ ms, and duration ~ 14 min.[34]

As prescribed by the "minimal preprocessing" protocols for BOLD data, the following spatial operations were performed: gradient distortion correction, rigid-body realignment, field-map processing and brain masking; it was decided to avoid using ICA-FIX denoised images due to the potentially complex effect of this filtering method on non-linear signal features.[35]

For the purpose of spatial normalization and segmentation of tissue compartments, a volume T_1-weighted 3D series was also acquired, having $TR = 2400$ ms, $TI = 1000$ ms, $TE = 2.1$ ms, flip angle $= 8°$, 224×224 mm field-of-view, and 0.7 mm isotopic voxel size. This volume was segmented using the SPM8 software.[36]

To avoid biasing subsequent analyses, very slow and potentially large fluctuations of implausible neural origin (coil heating, electronics drifts, head movement, etc.) were removed from all BOLD time-series by fitting an order-4 polynomial. Subsequent temporal filtering steps reflect the different requirements of linear (graph-based connectivity modelling, Fourier amplitude measurement) and non-linear analyses (correlation dimension).

B. Data analysis: Linear analyses

For linear analyses, low-pass filtering was applied through a Butterworth bank of order 4 and $f_{-3\,\mathrm{dB}} = 0.35$ Hz (i.e., half the Nyquist frequency). The 6 head movement vectors (3 translation and 3 rotation), their first temporal derivative and the average signal in white matter (segmentation threshold 0.9) and in ventricles were then removed by linear regression; prior to entering the regression, these nuisance time-series were temporally filtered as above. Spatial smoothing with a Gaussian kernel having half-maximum width of 6 mm was performed, then the time-series were rescaled to relative change with respect to mean voxel intensity and the temporal standard deviation σ was measured to quantify overall BOLD fluctuation amplitude.

Node degree, thereafter referred to with k and rescaled to unity integral, was calculated by linear correlation across all pairs of brain voxels (approx. 2×10^5), adaptively determining the correlation threshold to yield a fixed network completeness of 2.5%; an optimized parallel implementation of linear correlation in C code provided in Ref. 37 was utilized.

The relative amplitude of low-frequency fluctuations, representing a commonly used index of BOLD spectral content, was calculated in relative terms dividing the average of magnitude Fourier amplitudes in the 0.005–0.1 Hz range by that for the 0.1–0.3 Hz range, i.e., as $\langle Y|0.005\text{–}0.1\mathrm{Hz}|\rangle / \langle Y|0.1\text{–}0.3\mathrm{Hz}|\rangle$; this approach was preferred to determination of the spectral scaling exponent β as it is more parsimonious with respect to assumptions on the underlying distribution.[19,28]

C. Data analysis: Correlation dimension and non-stationarity

Non-linear analysis was performed, independently for each voxel time-series, using the TISEAN software version 3.0.1 (Max-Planck-Institut für Physik komplexer Systeme, Dresden, Germany), maintaining default settings unless otherwise specified.[38–40] This particularly computationally demanding analysis was run partially on a Linux computing cluster at the University of Trento and partially on an in-house Cray XD1 system (Cray, Inc., Seattle, WA, USA). For this analysis, following Ref. 41, we refrained from applying temporal low-pass filtering (which would enhance autocorrelation) or removing linear covariance with movement vectors and tissue-average signals; spatial smoothing as indicated above had to be retained to attain sufficient signal-to-noise ratio.

Instead, non-linear noise reduction was performed by means of orthogonal projection onto a 2-dimensional manifold using a special metric, setting embedding dimension $m = \tau/2$, where τ corresponds to the first minimum of the time-lag mutual information, determined as indicated below.[42,43] Prior to this operation, to avoid bias in subsequent surrogate generation, time-series were windowed minimizing zeroth- and first-order end-to-end mismatch power (resulting median length 1080 points).[38–40] After filtering, surrogate time-series were generated using an iterative method which largely preserves temporal autocorrelation and value distribution, by iteratively filtering towards the desired Fourier amplitudes and rank-ordering the value distribution.[44] All subsequent operations were performed identically and independently on the measured and surrogate time-series.

Time-delay embedding in $\mathbf{y}(t) = [y(t), \ y(t+\tau)\ldots y(t+(m-1)\tau)]$ was performed.[45] Embedding delay τ was determined as the first minimum of the time-lag mutual information, searching within ±20 frames to reject shallow local minima.[46] Embedding dimension m was then chosen applying the false nearest neighbours method, empirically setting escape factor of 6 and iteratively increasing dimension until there were <5% false nearest neighbours or higher dimensions could not be calculated due to lack of neighbours.[47] The effect of temporal autocorrelation was reduced by assuming a Theiler window w corresponding to the first maximum of the average space-time separation plot.[48,49]

The correlation dimension curves $D_2(m,\varepsilon)$, representing the local slopes of the correlation sum $C(m,\varepsilon)$, were thereafter calculated by means of an efficient box-assisted search implementation of the Grassberger-Procaccia algorithm, for embedding dimensions 1 to $2m$ (overembedding).[38–40,50] As the large number of time-series rendered visual inspection of the $D_2(m,\varepsilon)$ curves impractical, the scaling range $[\varepsilon',\varepsilon'']$ was determined automatically using sequential quadratic programming according to the following two procedures. These additional processing steps were completed using scripts developed in-house in the MatLab language (MathWorks, Inc., Natick, MA, USA) and freely available upon request.

Procedure #1 had two degrees of freedom and consisted of maximising the F-value for a horizontal segment between length scales $[\varepsilon',\varepsilon'']$, subject to the constraints $\log(\varepsilon'') - \log(\varepsilon') \geq 1$, $\log(\varepsilon'') - \log(\varepsilon') \leq 3$, $\varepsilon'' \leq \max[\varepsilon]$, $\varepsilon' \geq \min[\varepsilon]$ (representing the intersection of the ε ranges of all D_2 curves). To improve convergence, 20 restarts were performed from log-equispaced segments between $\min[\varepsilon]$, $\max[\varepsilon]$, and $D_2(m,\varepsilon)$ curves were smoothed with a $n = 10$

median filter. To investigate saturation of $D_2(m,\varepsilon)$ with embedding dimension m, this procedure was applied to the overembedding range $[m,2\,m]$, yielding D_2 and δD_2, representing, respectively, the median D_2 value in the chosen scaling range and the corresponding 5%–95% confidence interval of D_2 points from all curves; homologous measures for the surrogates are referred to with $\hat{D}_2$ and $\delta\hat{D}_2$.

Procedure #2 had only one degree of freedom and implied a fixed scaling range length assumption, $\log(\varepsilon'') - \log(\varepsilon') = 1.4$, predicated on the median segment length obtained with procedure #1. This procedure minimized the median span of D_2 values observed across the (over)embedding dimensions $[m,2m]$ within the selected scaling range. The same curve smoothing and restarts as above were applied, and resulting median and confidence intervals are referred to as D'_2 and $\delta D'_2$ for the measured time-series, $\hat{D}'_2$ and $\delta\hat{D}'_2$ for the surrogates; the constraints were $\log(\varepsilon'') \leq -1$, reflecting the fact that above this length scale D_2 curves decayed rapidly, and $\log(\varepsilon'') - 1.4 \geq \mathrm{med}\{\min[\log(\varepsilon)]\}$, representing the shortest length scale for which at least half of curves were defined.

For stationary and purely stochastic BOLD activity, no systematic difference is expected between measured time-series and Gaussian linear surrogates. On the other hand, in the presence of an underlying self-similar attractor, one expects only for the measured time-series some evidence of saturation of $D_2(m,\varepsilon)$ in the overembedding range $[m,2m]$, from which $D_2 < \hat{D}_2$ and $\delta D_2 < \delta\hat{D}_2$.

Fourier surrogates do not represent non-stationarity effects and systematic difference with respect to measured time-series may therefore be driven by non-stationarity rather than non-linearity.[38] To informally test for inhomogeneous non-stationarity across cortical regions, the unfiltered time-series were subdivided in segments and the normalized median cross-forecast error (CFE) based on a locally zeroth-order model was calculated.[51] The embedding dimension was fixed to 4 and two settings were considered: $\# = 12$ segments with $\tau = 10$ frames, and $\# = 6$ segments with $\tau = 20$ frames. The former yielded a segment length of $\approx$70 s, comparable with sliding window lengths previously found to be associated with strong dynamical fluctuations of connectivity;[22] the latter preserved embedding delay closer to the median for gray matter voxels.

D. Data analysis: Topographical correlation

For correlation with node degree, the differences, $\hat{D}_2 - D_2$ and $\delta\hat{D}_2 - \delta D_2$ (procedure #1), $\hat{D}'_2 - D'_2$ and $\delta\hat{D}'_2 - \delta D'_2$ (procedure #2), were therefore considered, representing two empirical measures of non-linear structure, expected to be positive in the presence of an underlying attractor leading to saturation of $D_2(m,\varepsilon)$ with increasing embedding dimension m. Varying levels of temporal autocorrelation are present in BOLD time-series and determinism is weak; hence, we strictly refrained from considering D_2, δD_2, D'_2, and $\delta D'_2$ values directly. We also correlated the CFEs, relative amplitude of low-frequency fluctuations, and BOLD% fluctuation amplitude σ with node degree.

To improve anatomical contrast, parametric maps from non-linear analysis were filtered with a $n = 3$ median filter. All individual parametric maps were then warped to 2 mm Montreal Neurological Institute (MNI) space using SPM8 and applying the normalization transformation determined from a reference volume acquired at the beginning of each series.[36] Median maps over 10 participants and 2 phase encoding directions were generated and Spearman rank-order correlations were calculated over 349 automatically generated cortical regions intersected with the group average gray matter segmentation map (segmentation threshold of 0.3) and having approximately homogeneous volume (2.5 ± 0.4 ml, median ± inter-quartile range, indexing an intermediate level of anatomical detail).[16] Given the clinical and demographic homogeneity of the sample, inter-individual correlations were not evaluated. For anatomical interpretation of the results, reference was made to the Mai, Paxinos, and Voss atlas.[52] Only for generating 3D cortical renderings (Figure 1), a further $n = 3$ median filtering step was applied to the group maps, and the white matter was masked out.

III. FUNCTIONAL MRI RESULTS

A. Linear analyses: Functional connectivity and low-frequency fluctuations amplitude

Node degree of functional connectivity (k, Figure 1(a)) was consistently high in (i) precuneus, with extension to the posterior cingulate cortex and cuneus, (ii) lateral parietal cortex, involving the angular gyri and inferior parietal lobules with extension to the supramarginal gyrus, and (iii) medial prefrontal cortex, involving its ventral and dorsal parts. Diffusely high node degree was also observed in the middle and inferior frontal gyri. Node degree was lowest in the paracentral lobule, extending along the precentral and postcentral gyri and occipital poles. The distribution of node degree was overall symmetric between the hemispheres.

The topographical heterogeneity of node degree was reflected in the relative amplitude of low-frequency fluctuations $(\langle Y|0.005\text{–}0.1\,\mathrm{Hz}|\rangle / \langle Y|0.1\text{–}0.3\,\mathrm{Hz}|\rangle$, Figure 1(b)): intense synchronization was strongly associated to a shift from white noise-like spectrum towards predominance of low-frequency fluctuations ($\rho = 0.92$, $p < 0.001$, Figures 2(a) and 2(b)), corresponding to stronger temporal autocorrelation.

Across regions, there was a marked negative correlation between node degree and temporal standard deviation of the BOLD time series ($\rho = -0.42$, $p < 0.001$), which allowed excluding the trivial hypothesis that the observed effects were simply consequential to larger fluctuations in the high-degree regions, leading to higher relative contribution of noise in the others.

B. Non-linear analysis: Correlation dimension and non-stationarity

Across regions, intense synchronization was also associated with clearer evidence of non-linear structure, obtained comparing correlation dimension estimates for measured and surrogate time-series. In higher-node degree areas, the

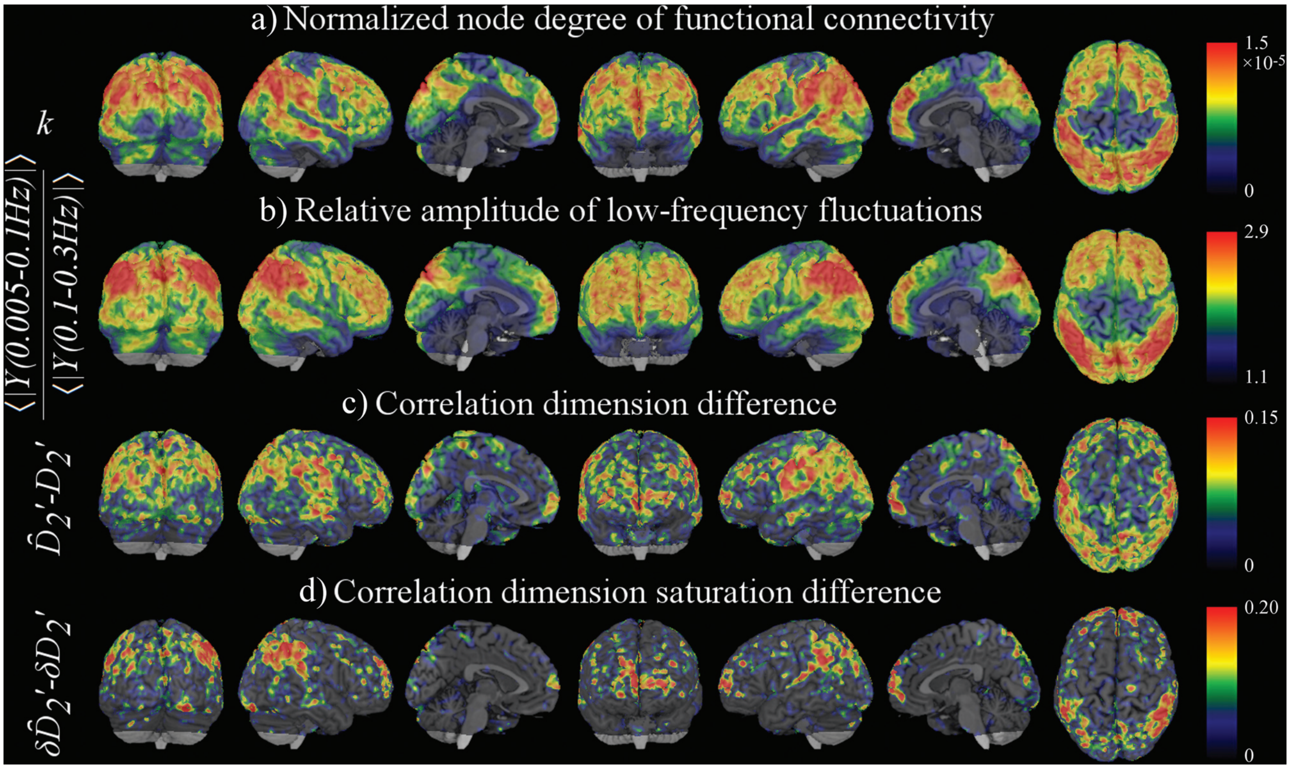

FIG. 1. Three-dimensional renderings on canonical brain surface depicting the group median distribution of (a) node degree of resting-state functional connectivity, representing pair-wise synchronization of BOLD time-series (k, normalized to unity integral); (b) mean Fourier amplitude of low- relative to high-frequency fluctuations $\langle Y|0.005-0.1\text{Hz}|\rangle/\langle Y|0.1-0.3\text{Hz}|\rangle$; (c) correlation dimension difference with respect to temporal autocorrelation- and value distribution-matched surrogate data $\hat{D}'_2 - D'_2$; (d) correlation dimension saturation difference, similarly reported as $\delta\hat{D}'_2 - \delta D'_2$. Only positive values are shown. Areas of intense functional connectivity (a) are characterized by larger low-amplitude fluctuations (b) and clearer evidence of saturation of $D_2(m,\varepsilon)$ curves with embedding dimension, pointing to presence of non-linear structure ((c) and (d)). See Sec. II C for further details.

median correlation dimension from measured time-series was more markedly lower compared to surrogates, irrespective of the estimator used (*Procedure #1*, $\hat{D}_2 - D_2$: $\rho = 0.52$, $p < 0.001$; *Procedure #2*, $\hat{D}'_2 - D'_2$: $\rho = 0.55$, $p < 0.001$, Figures 1(c) and 2(c)). Similarly, in higher-node degree areas, the correlation dimension curves $D_2(m,\varepsilon)$ saturated to a tighter plateau in the over-embedding range $[m,2m]$ compared to surrogates, irrespective of the estimator used (*Procedure #1*, $\delta\hat{D}_2 - \delta D_2$: $\rho = 0.35$, $p < 0.001$; *Procedure #2*, $\delta\hat{D}'_2 - \delta D'_2$: $\rho = 0.52$, $p < 0.001$, Figures 1(d) and 2(d)). While correlation dimension differences between measured and surrogate time-series were quantitatively small, warning of weak determinism, they were clearly consistent across voxels in given regions and across participants, as confirmed by the robust topographical correlations observed on the group median maps, on which lateral parietal and medial frontal regions were particularly well-delineated.

The CFE calculated over 12 segments was not correlated with node degree ($p = 0.3$); however, there was a very strong negative correlation between the CFE calculated over 6

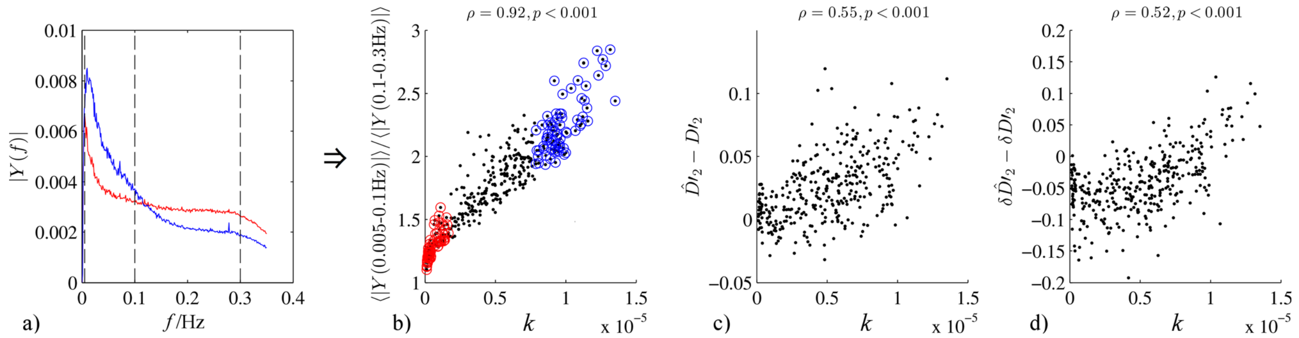

FIG. 2. (a) Normalized average amplitude spectra from voxels in the 20% least (red) and most (blue) connected regions, showing increased relative low-frequency content for the latter. (b) Scatter plot of relative low frequency activity amplitude $\langle Y|0.005-0.1\text{Hz}|\rangle/\langle Y|0.1-0.3\text{Hz}|\rangle$ vs. node degree k, normalized to unity integral. (c) Scatter plot of correlation dimension difference with respect to temporal autocorrelation- and value distribution-matched surrogate data $\hat{D}'_2 - D'_2$ vs. node degree k; (d) corresponding scatter plot for correlation dimension saturation $\delta\hat{D}'_2 - \delta D'_2$. Across cortical regions, high node degree was significantly associated to larger relative amplitude of low-frequency activity ($\rho = 0.92$) and clearer saturation of the $D_2(m,\varepsilon)$ curves with embedding dimension, visible as lower median correlation dimension ($\rho = 0.55$) and a tighter plateau ($\rho = 0.52$) with respect to the surrogates. See Sec. II C for further details.

segments and node degree ($\rho = -0.90$, $p < 0.001$). This finding suggested stronger action of deterministic dynamics in high-node degree areas and allowed arguing against greater non-stationarity which could have selectively biased comparison with surrogates. Example time-series for representative high- and low-node degree regions are shown in Figure 3.

IV. SINGLE-TRANSISTOR OSCILLATOR NETWORK METHODS

A. Network topology

In an attempt to recreate experimentally the relationship between connectivity and non-linear dynamics observed for the brain in a different physical system of much smaller topological scale, a network of diffusively coupled single-transistors oscillators was realized. This consisted of a ring of 90 nodes, to which long-distance links were added to create four approximately equi-spaced "hub" regions: three smaller hubs, consisting of 3 nodes each (red, green, and blue in Figure 4(a)), were wired to a larger hub consisting of 9 nodes (yellow). The order of incidence of the long-range connections in the larger hub was intermixed, in an analogy to the fact that in densely connected brain regions like the precuneus synapses with distant cortical areas (such as the lateral parietal and medial prefrontal cortices) are formed in a deeply intertwined manner.[53]

B. Oscillator circuit

The chaotic circuit (Figure 4(b)) consisted of an NPN bipolar-junction transistor connected to two inductors and a capacitor in a Hartley-similar configuration, i.e., with an LC series network (C1-L1) between collector and emitter, and an inductor (L2) between collector and base. This autonomous oscillator, described in detail in Ref. 31, is powered from a 5 V DC voltage source through a variable resistor (R1) and was realized using off-the-shelf transistors (2N2222A), inductors of nominal values 8.2 μH (L1) and 10 μH (L2), and capacitors of nominal value 30 pF (C1). It generates chaotic signals having approximately stable periodicity but highly variable cycle amplitude and is easily synchronized via resistive coupling at the collector node.[32] Due to the presence of multiple LC networks instanced not only by the discrete components but also by stray capacitances, junction capacitances, and other effects, diverse resonance frequencies are available; while R1 is varied different oscillation modes are visited, and chaos can ensue through quasiperiodicity.[26,27,31] By tuning R1, it is possible to obtain oscillation that is chaotic irrespective of coupling with other oscillators or periodic but close to phase transition to chaos. This enables exploring the hypothesis that certain collective phenomena appear preferentially close to the point of criticality, as found for the emergence of functional from structural connectivity in some simulations of brain dynamics.[5–7,9,10]

C. Network implementation

The ring was materially constructed by cascading three STRANGE-1 boards (Figure 4(c)), each harbouring 30 oscillators, which were used in a recent study where formation of complex community structure was demonstrated and where the addressing and readout circuitry is described in greater detail.[32] Here, to allow cascading the three boards, the initial chain consisting of an OPA633KP video buffer (Texas Instruments, Inc., Dallas, TX, USA) and DG506B multiplexer (Vishay Electronic GmbH, Selb, Germany) was extended with LT1227 addressable buffers (Linear Technology, Inc., Milipitas, CA, USA); with respect to Ref. 32, the present setup also included attenuation by a factor of 2 to reduce slew rate and limit parasitic low-pass filtering effects.

Following preliminary experiments, the coupling resistance between neighbours (R2 and R3 in Figure 4(b)) was set

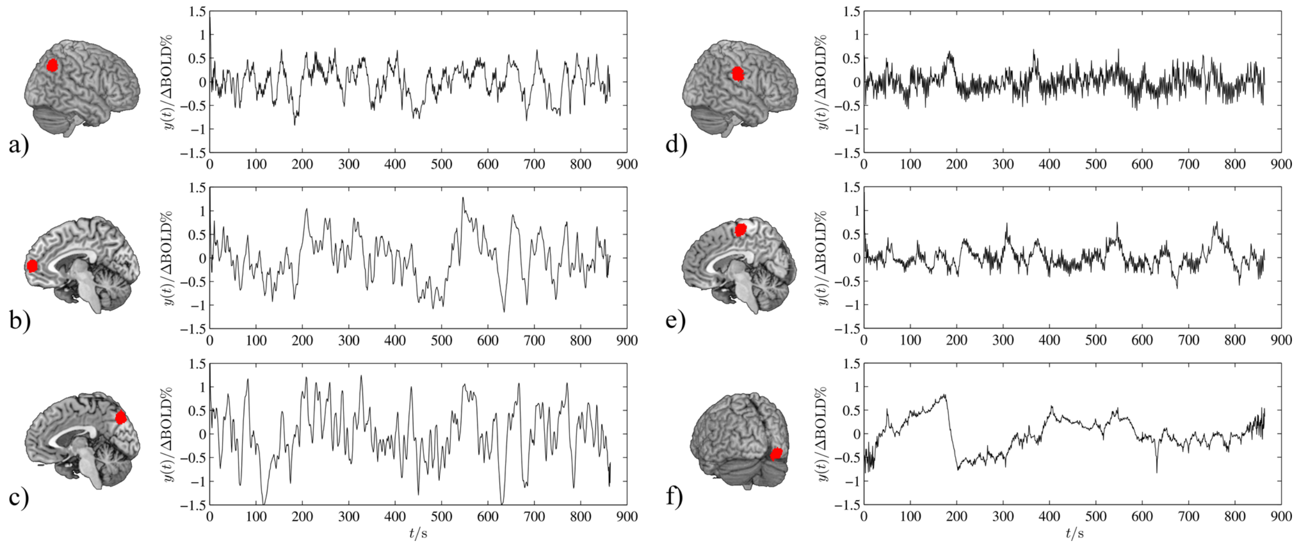

FIG. 3. Example average BOLD time-series ($y(t)$, expressed as percent change) from an arbitrarily chosen resting-state fMRI session for three representative high-node degree ((a) angular gyrus, (b) medial prefrontal cortex, and (c) precuneus) and low-node degree ((d) pre/post central gyri, (e) paracentral lobule, and (f) occipital pole) regions. Time-series were extracted from 4 ml spheres intersected with the parenchyma and filtered as described in Sec. II C. Increased regularity of BOLD fluctuations in the high-node degree regions is clearly noticeable.

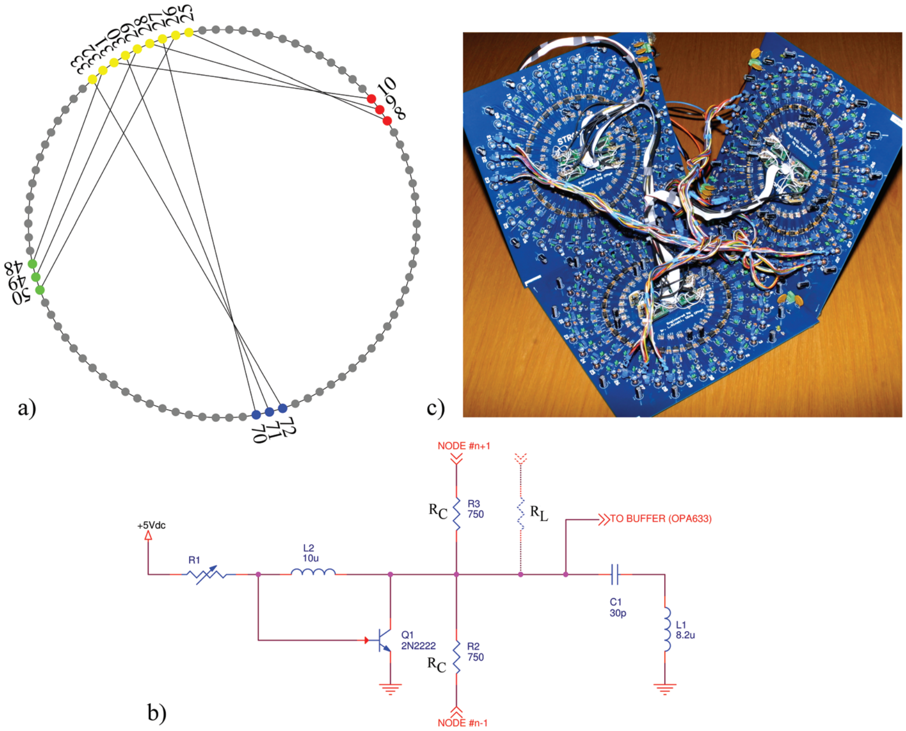

FIG. 4. (a) Network topology for oscillator coupling, including long-distance links establishing nodes 8–10 (red), 48–50 (green), and 70–72 (blue) and nodes 25–33 (yellow) as "extended hubs," representing an analogy to the highly connected cortical regions. (b) Circuit diagram of the chaotic oscillator, where R1 is the DC voltage source series resistor, R2 and R3 implement coupling with neighbouring nodes (value set to R_C), and the dashed resistor (value set to R_L) represents the long-distance link instanced only for nodes in the hub regions. (c) Experimental setup, based on three STRANGE-1 boards[32] with additional wiring for node addressing during readout and long-distance connections.

to $R_C = 750\ \Omega$, which allows diffusion of synchronization over intermediate distances (see Figure 5) and represents an intermediate value in the range considered in Ref. 32. Measurements were conducted with R1 (DC voltage source series resistor) set for chaotic oscillation or periodic oscillation close to the point of criticality; to obtain the desired oscillation mode irrespectively of component tolerances, R1 could not be set uniformly but was iteratively tuned in random node order with $R_C = R_L = \infty$. Resulting values were median 1180 Ω (range 410 Ω, 1960 Ω) for chaotic oscillation and 790 Ω (390 Ω, 1620 Ω) for periodic oscillation close to the point of criticality. These intervals do not closely align to

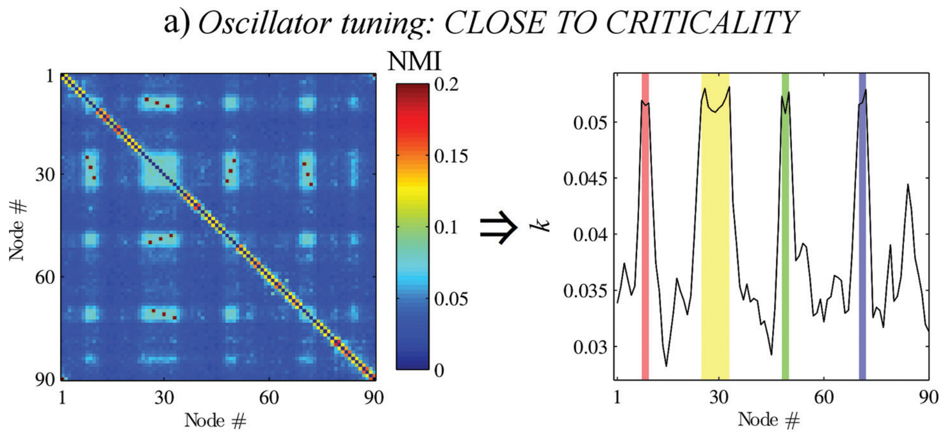
a) *Oscillator tuning: CLOSE TO CRITICALITY*

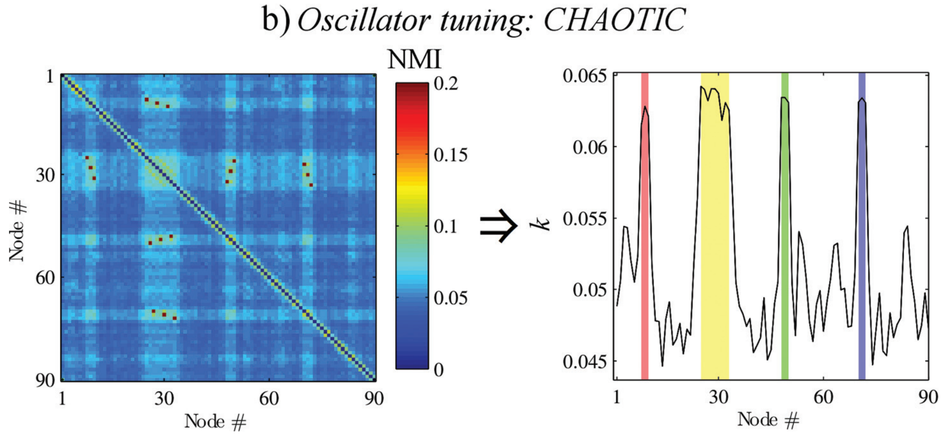
b) *Oscillator tuning: CHAOTIC*

FIG. 5. Weighted adjacency matrices and corresponding average synchronization k for oscillators tuned (a) close to criticality and (b) chaotically. The long-distance structural links ($R_L = 40$ Ω) created "islands" of synchronization among the hub regions and increased their average synchronization. Red, yellow, green, and blue shading corresponds to nodes 8–10, 25–33, 48–50, and 70–72, respectively (see Figure 4(a) for network diagram).

Ref. 31 principally due to inter-oscillator coupling, parasitics in the variable resistor, and loading by the buffer amplifier.

The coupling resistance for long-distance links was empirically set to $R_L = 40\ \Omega$; this low value accounted for the fact that observed synchronization strength for a given resistance was significantly weaker for distant nodes than neighbours, plausibly due to radiation by the 60 cm-long coupling cable, which consisted of ten 0.9 mm isolated wires connected in series to 2.2 nF capacitors at each end, providing a self-resonance frequency ∼ 8.5 MHz. Additional measurements were performed with $R_L = 80\ \Omega$ and 160 Ω.

D. Data acquisition

To eliminate the possibility of bias due to inherent differences between nodes unrelated to connectivity, 6 acquisitions were performed for each condition, rotating the network graph along the physical ring to change the physical nodes corresponding to each hub, while maintaining the relative locations of the nodes on the "logical" graph unvaried. Six rotations were performed, assigning the larger (yellow) hub to physical nodes 5–13, 25–33, 35–43, 55–63, 65–73, and 85–3.

Waveforms were recorded in 100 μs (50 000 points) windows at 500 MSample/s 8-bit precision using an LC534AM oscilloscope (LeCroy, Inc., Chestnut Ridge, NY, USA) equipped with ×10 field-effect transistor active probes minimizing distortion (AP020, LeCroy Inc.). There were approximately 60–70 time-points per cycle. Gain and offset were set to 200 mV/div and − 300 mV, with AC coupling and 25 MHz bandwidth limiting. The complete datasets are available upon request.

The experiment was controlled through a script running under MatLab 2012a (MathWorks, Inc., Natick, MA, USA), which ran on a Linux host and was interfaced to the oscilloscope via IEEE488 and to the readout multiplexers via RS232. Each acquisition consisted of 1980 runs in random order, each one simultaneously sampling four addressed nodes.

E. Data analysis

To determine synchronization of cycle amplitude fluctuations as in Ref. 32, waveforms were smoothed through a running average window over 6 ns (3 samples) and local maxima were extracted over a 60 ns (30 samples) window. Corresponding values were interpolated via cubic spline and synchronization was quantified by means of normalized mutual information, defined according to

$$NMI_{ij} = I_{ij}/\sqrt{H_i H_j},$$

where H_i and H_j represent the entropies of time-series from nodes i and j, and I_{ij} their mutual information.[54,55] The average synchronization of each node was calculated with $k_i = \sum_{j=1}^{90} NMI_{ij}/90$; this approach, common in literature on weighted networks, was preferred to canonical node degree as it does not involve assumptions for graph binarization.[56]

The relative amplitude of low-frequency oscillations was measured similarly to BOLD data, but in this case as the average absolute Fourier amplitude in the 0.3–1.9 MHz range with respect to the 1.9–3.5 MHz range; these ranges were empirically chosen as cycle amplitude fluctuations for nodes outside the hub regions peaked at ∼1.9 MHz (see Sec. V A).

To avoid autocorrelation effects introduced by interpolation, the correlation dimension was calculated directly on the recorded time-series using the same methods as for the BOLD signal rather than on interpolated cycle amplitude (see Sec. II C), but setting for *Procedure #2* $\log(\varepsilon'') - \log(\varepsilon') = 1.5$, $\varepsilon'' \leq \max[\varepsilon]$, and $\varepsilon' \geq \min[\varepsilon]$ and minimizing directly the overall 5%–95% confidence interval. To limit computational load, time-series were truncated at 25 000 points; further, while during each acquisition 88 time-series were recorded for each node, non-linear analysis was performed only for 10 per node, and the median was taken over the 10 time-series and 6 graph rotations.

V. SINGLE-TRANSISTOR OSCILLATOR NETWORK RESULTS

A. Synchronization and low-frequency content of cycle amplitude fluctuations

Long-distance structural links increased synchronization (functional connectivity) among the hub regions and obliterated smaller clusters which formed spontaneously. Close to criticality as well as with chaotic oscillation, these links created "islands" of synchronization among the hub nodes and pervasively increased synchronization between them and the entire network (Figure 5); this bears an immediate analogy to the effect of structural connectivity on functional connectivity in the brain. The consequence was a marked increase in average synchronization k for the hub regions, which was statistically significant with both oscillator settings (supplementary Table I;[57] $p < 0.001$).

For oscillation close to criticality and in the absence of long-distance structural links, cycle amplitude fluctuations were small and plausibly related primarily to frequency mismatch between the nodes; by contrast, large low-frequency fluctuations arose in the hub regions, suggesting that the long-distance links locally caused transition to chaos (Figure 6). When the DC voltage series resistance (R1) was set for chaotic oscillation, as expected global chaoticity was observed over the entire ring irrespective of connectivity (traces not shown).

In both conditions, the spectral content of cycle amplitude fluctuations depended on connectivity. Close to criticality, for nodes outside the hubs, most power was concentrated around ≈1.9 MHz, with a $1/f^{\beta}$-like tail observed at much lower frequencies; by contrast, analogously to observations for the brain, inside the hub regions activity shifted towards ≈1 MHz (Figure 7(a)). Albeit at slightly different frequencies, a similar effect was observed for globally chaotic oscillation (Figure 7(b)). The graded relationship between regional synchronization and relative low-frequency amplitude observed for the brain was found also here, in that increasing the long-distance link coupling resistance brought about a correspondingly weaker frequency shift (the amplitude ratio inside the hub regions was 4.2, 2.4, and 1.6 for $R_L = 40$, 80, and 160 Ω, respectively, see supplementary Table I[57]).

TABLE I. Conceptual comparison of the *in-vivo* and *in-silico* experiments: despite profound physical and scale differences (points #1-#7), the systems share two key structural and dynamical aspects (points #8 and #9) leading to a consonant observation (point #12).

Nos.		*In-vivo* experiment	*In-silico* experiment
1	System type	Biological (electrochemical), natural	Analog electronic, artificial
2	Network size	≈200 000 nodes (voxels), each representing ≈10^5–10^7 neurons	90 nodes (discrete oscillators)
3	Oscillators	Non-identical (after neuron phenotype, local biochemical environment, etc.)	Non-identical (after manufacturing tolerances in inductors, capacitor, and transistor)
4	Measured variable	Ensemble average neural activity, convolved with hemodynamic response (via fMRI scanning)	Voltage (via active oscilloscope probe)
5	Spatiotemporal scale	μm, ms (observed scale: mm, s)	cm, μs
6	Time-series length	1200 points (864 s, 1.4 Sa/s)	50 000 points (100 μs, 500 MSample/s)
7	Coupling mechanism	Unidirectional, non-linear, delayed, and refractory (synapses)	Linear diffusive, instantaneous (resistors)
8	Operating point	Widely hypothesized to be close to criticality following evolutionary adaptation	Manually tuned close to criticality via DC voltage source series resistors
9	Connectivity topology	Adaptive, abundant short-range connections (i.e., "U-fibres" among nearby cortical regions) supplemented with fewer long-range connections (i.e., association and projection fibres) hinged around preferentially interconnected "hub" cortical regions	Hardwired, abundant short-range connections (i.e., links between neighbours according to ring topology) supplemented with fewer long-range links, forming four preferentially interconnected "extended hub" regions
10	Activity in weaker-connected regions	Seemingly stochastic	Periodic
11	Activity in "hub" regions	Possibly chaotic	Chaotic
12	Observed correlation dimension (D_2)	Lower and saturating to a tighter plateau with respect to surrogates in the known "hub" cortical regions compared to the others	Lower and saturating to a tighter plateau with respect to surrogates in the hardwired "extended hub" regions compared to the other nodes

B. Correlation dimension

As observed for the brain, intense functional connectivity (average synchronization) was associated with greater evidence of non-linear structure. When the oscillators were tuned close to criticality, for nodes within the hub regions compared to the others, the correlation dimension was more markedly lower than the surrogates and the corresponding curves converged to a tighter plateau in the over-embedding range [m,2m] (Figure 7(a)); both effects were statistically

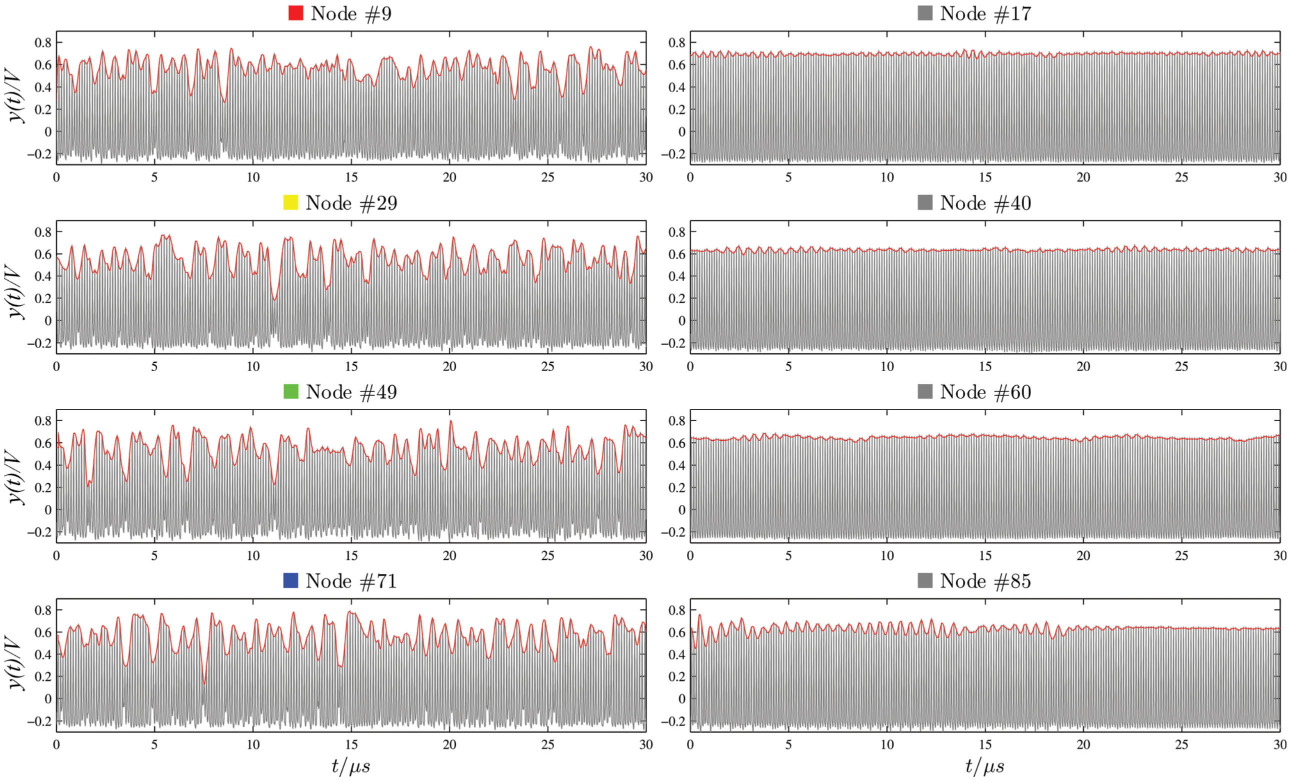

FIG. 6. Continuous signal (gray) and interpolated cycle amplitude (red) for representative nodes, having DC voltage series resistance set for periodic oscillation close to criticality, with (#9, 29, 49, 71) and without (#17, 40, 60, 85) long-distance links ($R_L = 40\ \Omega$). In the hub regions, chaoticity was manifest as large, low-frequency cycle amplitude fluctuations, whereas outside cycle amplitude was approximately constant (periodic oscillation).

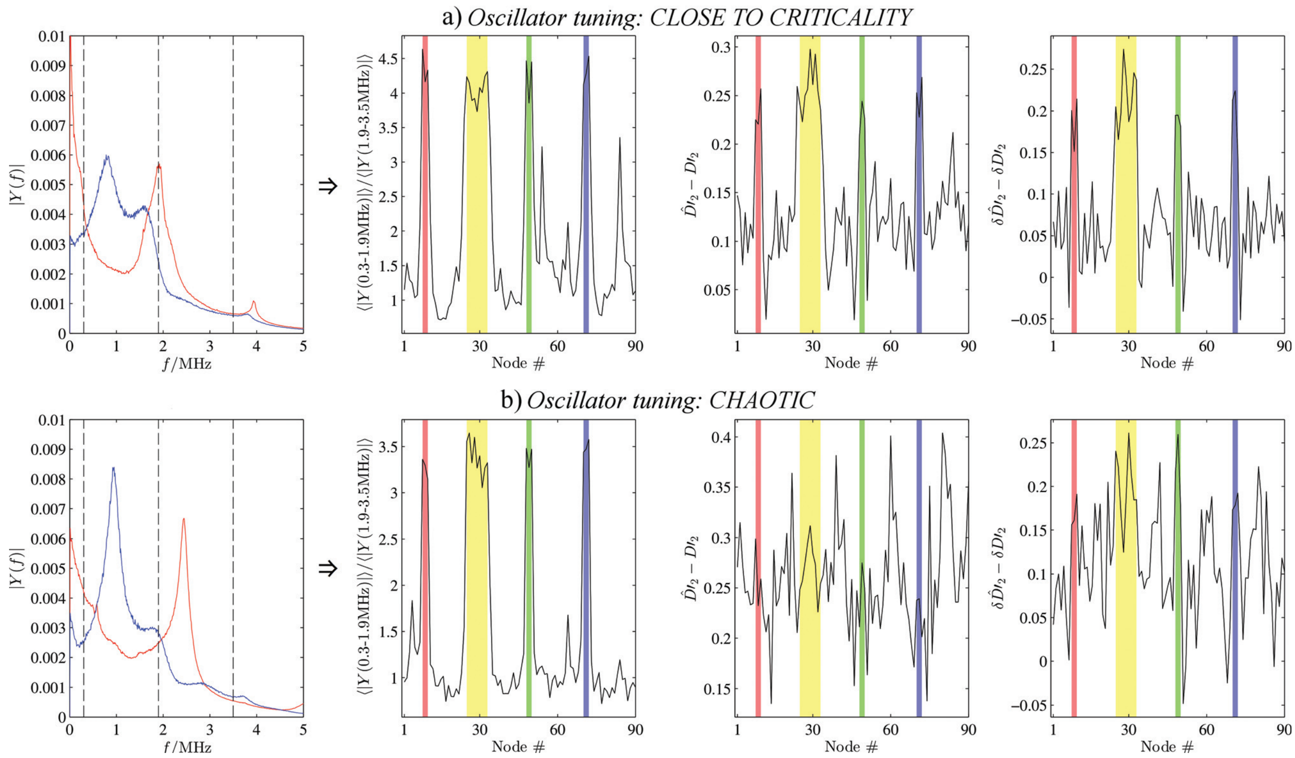

FIG. 7. Spectral and non-linear dynamical measures for oscillators tuned (a) close to criticality and (b) chaotically. From left to right: (i) Normalized average amplitude spectra from nodes with (blue) and without (red) long-distance links, demonstrating shift to lower frequency activity in the hub regions; (ii) corresponding plot of relative average Fourier amplitude of low-frequency fluctuations; (iii) correlation dimension difference with respect to temporal autocorrelation- and value distribution-matched surrogate data $\hat{D}'_2 - D'_2$, (iv) correlation dimension saturation difference, similarly reported as $\delta\hat{D}'_2 - \delta D'_2$. Red, yellow, green, and blue shading corresponds to nodes 8–10, 25–33, 48–50, and 70–72, respectively (see Figure 4(a) for network diagram). In the hub regions, increased relative intensity of low-frequency activity is observed, alongside lower median correlation dimension saturating to tighter plateau with respect to the surrogates ($p < 0.001$ for all comparisons in (a), see supplementary Table I[57] for details); the effect is stronger close to criticality.

significant irrespective of the estimator used (supplementary Table I;[57] $p < 0.001$) and represented the fact that phase randomization had a greater impact on the chaotic time-series than on the periodic ones, as the latter had much more concentrated spectral content. The correlation dimension for the measured time-series (considered also directly here in virtue of the stronger determinism with respect to the brain time-series) was markedly higher for nodes inside (median 1.8; range 1.8, 1.9) than outside (1.3; 1.1, 1.5) the hub regions (supplementary Table I;[57] $p < 0.001$), providing further evidence of transition to chaos.

When the oscillators were chaotically tuned, the correspondence between connectivity and non-linear structure became much weaker (Figure 7(b)): for nodes inside compared to outside the hubs, the correlation dimension curves still converged more tightly with respect to surrogates, but there was no significant difference in the correlation dimension (supplementary Table I[57]). This implies that the effect of connectivity on non-linear dynamics was stronger when the system was tuned close to criticality.

VI. DISCUSSION

A. Correspondence between synchronization, spectral content, and non-linear dynamics in resting-state brain activity

While spatiotemporal coherencies underlying RSNs are knowingly driven by low-frequency activity <0.1 Hz, in itself, this does not imply that the intensity of these fluctuations is topographically related to "overall strength" of functional connectivity (activity synchronization), particularly given that using approaches like independent component or seed-based analysis discrete anti-correlated or even asynchronous RSNs are found.[7,11,12,22,58] Using a graph-based model of inter-regional synchronization, we were able to show strong coupling between node degree and relative amplitude of low-frequency activity, more explicitly than previous studies which considered individual RSNs rather than a holistic representation of the functional connectome.[59,60] Spontaneous brain activity during awake idleness generates BOLD signals that have approximately white noise-like spectrum for weakly connected (synchronized) regions and display a gradual shift towards low-frequency fluctuations (e.g., pink, red or brown noise), corresponding to increased temporal autocorrelation, in stronger-connected areas such as precuneus, lateral parietal, and medial frontal cortex. The observed distributions of node degree and relative Fourier amplitude of low-frequency activity are in close agreement with existing reports considering the two parameters separately and are unlikely to be driven primarily by noise.[13–16,18,28,29,37,61]

This spectral heterogeneity points to different dynamics of underlying neural activity. Even though BOLD signals are not well-suited for non-linear dynamical analysis due to short time-series length, undersampling, physiological noise, and confounds from neurovascular coupling, we attempted to generate voxel-based maps of the correlation dimension (D_2) which, with reference to surrogate data, yielded greater evidence of saturation with increasing embedding dimension in the highly synchronized regions. We conjecture that this result could present evidence of non-linear structure representing low-dimensional chaos emerging as a function of high connectivity, over a "baseline" of stochastic activity which is preponderant in low-connectivity regions.

Non-linear analyses were only interpreted in respect to identically and independently analyzed surrogate data, which allow making relatively unconfounded inferences of non-linearity even for noisy physiological time-series as in Ref. 62, irrespective of the specific non-linear measure chosen;[38] furthermore, two different D_2 determination procedures (having one or two degrees of freedom) were found to yield convergent findings, consistent across participants and voxels. Nevertheless, this inference of non-linear structure should be interpreted cautiously due to weak determinism compared to other studies conducted on other, non-biological physical systems yielding longer, more densely sampled and less noisy time-series representing a more favourable scenario for non-linear analysis, such as in Ref. 63.

Our findings are well in line with the previous studies which had already established that the temporal fluctuations in BOLD time-series cannot be fully attributed to linear stochastic processes and suggested the action of low-dimensional chaotic attractors. However, to the authors' knowledge, existing studies considered either a small set of voxels from predetermined regions of the visual cortex or spatiotemporal decomposition and did not establish a topographical relationship with connectivity.[64,65]

B. Source(s) of low-frequency BOLD activity

Neural events unfold on the scale of milliseconds and the mechanisms underlying generation of spatiotemporally correlated scale-free-like activity including significant power at <0.1 Hz remain incompletely understood.[19] It is generally agreed that they represent the lowest-frequency end of broad spectra (equivalently, amplitude envelope of much higher frequency oscillations) generated by collective non-linear neural dynamics, which emerge either spontaneously or tracking external sensory stimulation, and are filtered through the hemodynamic response.[7,17,58] Low-frequency BOLD fluctuations are predicted to arise in a remarkably diverse set of simulation scenarios, comprehensively reviewed in Ref. 7, irrespective of whether regional activity is represented through realistic spiking models, mean-field models, or simplified systems such as Kuramoto and Wilson-Cowan oscillators. These models yield synthetic low-frequency BOLD time-series which, to varying accuracy levels, predict functional connectivity from structural connectivity through diverse dynamical phenomena including synchronization of chaotic activity, reverberation, metastability, and noise-induced exploration of "ghost" attractors.[7,8,30,66]

Our experimental observations of stronger low-frequency activity and non-linear structure in highly synchronized (high node degree) cortical areas, if confirmed with higher-temporal resolution techniques such as magnetoencephalography, may help set further constraints to the validity of these models beyond the prevalent Pearson coefficient-based comparison of functional connectivity matrices.[6–10,58] To our knowledge, across existing simulation studies elements of this correspondence have been reported heterogeneously. For example, in Ref. 66, it was demonstrated that, for an optimal parameter set, in a network of Wilson-Cowan oscillators slow fluctuations emerge in the level of synchronization between communities even when the activity of each neural population does not individually show this modulation, thus establishing an explicit mechanism coupling connectivity and low-frequency activity. In Ref. 8, Kuramoto oscillators with weak and delayed coupling, having a working point such that synchronization is limited to clusters but not global, were found to generate large fluctuations in the frequency range that the BOLD signal can track through hemodynamic coupling; by contrast, regular activity with spectral power concentrated at higher frequencies leads to small and irregular BOLD fluctuations. In Ref. 67, meso-scale modelling of two neural populations reproduced substantial changes of spectral scale invariance as a function of excitatory/inhibitory input and density of long-range connections.

C. Analogy between brain and single-transistor chaotic oscillator networks

In this study, recourse to an experimental network of single-transistor chaotic oscillators enabled demonstrating an instance of causal relationship between connectivity and chaoticity, wherein insertion of long-distance links incident on extended hub regions locally resulted in emergence of chaos and generation of stronger low-frequency activity selectively for oscillators within the hubs. Supported by the evidence discussed above, we conjecture that a similar relationship could also hold true for the brain.

At least at face value, homology between the brain and chaotic oscillator findings is noteworthy. As summarized in Table I, there are profound differences between the two systems, particularly in terms of network size ($\approx 10^{11}$ neurons vs. $\approx 10^2$ nodes), complexity of connectivity (human connectome vs. ring with short-cuts), coupling mechanism (synapses vs. resistors), and temporal sampling; however, the two systems share the fact that some network regions are hard-wired as densely connected "hubs," and that nodes are tuned to operate close to criticality. It should also be noted that the chaotic oscillators generated signals at frequencies much higher than those recorded for the brain; while operation on the same temporal scale could have been desirable for ease of comparison, for the chosen circuit this would have implied impractically large values for the reactive components.

The relationship between connectivity and non-linearity was strongest when the single-transistor oscillators were tuned close to transition to chaos, recalling simulations of collective brain dynamics at criticality.[5,6,9] Though the spectral content was unavoidably different with respect to the

BOLD time-series and the frequency windows were, in both cases, determined arbitrarily rather than based on theoretical assumptions, the observed shift in spectral content toward lower frequencies depended on long-distance connection strength, clearly recalling the graded relationship found with respect to node degree in the brain.

On the basis of previous experimental investigations of this chaotic circuit, it appears plausible that quasiperiodicity effects are involved in the transition to chaos: as the experimental oscillators under consideration were non-identical due to large manufacturing tolerances, dynamical and spectral differences could induce activity at non-trivial frequency ratios. Owing to diffusive coupling and transistor non-linearity, coupled oscillators could mutually influence each other in a complex manner reflecting the absence of an invariant manifold.[68] Close to criticality, this can lead to chaos as also observed for other physical systems.[26,27] While the two variables were not independently manipulated in this experiment, the effect is plausibly related to node degree as well as topological distance. Coupling to a larger number of oscillators (3 instead of 2) generating non-identical spectra inherently promotes transition to chaos. At the same time, because in the absence of long-distance connections neighbouring oscillators tend to form extended synchronized communities, direct coupling with a distant node generating a highly uncorrelated signal is likely to have greater impact on dynamics than coupling with a closer node with respect to which activity is already partially synchronized.[32]

D. Relevance of experimental physical models and connectivity—Non-linear dynamics correspondence in other networks

Experimental physical modelling in analog electronic circuits has potential to play a complementary role with respect to numerical simulations of brain dynamics. Through the presence of complex non-idealities, device tolerances and dynamical noise experimental systems such as transistor oscillators readily capture the reality that networks of identical oscillators are never encountered in living organisms, while being inherently free from temporal and magnitude discretization.[68] Further, while in the present proof-of-concept study the network was realized with discrete components, much higher-density implementation in CMOS technology is possible and currently under development. As the number of nodes is elevated $\gg 10^2$, the level of computational complexity represented per area and power in analog circuits can vastly exceed the capability of realistic sequentially run numerical simulations.[69]

While more limited literature is available regarding the impact of network topology on chaoticity rather than on synchronization, indirect support for the view that chaos can ensue as a consequence of certain connectivity features is found throughout disparate reports.[68,70,71] Simulations of elementary systems and artificial neural networks under diverse scenarios highlight that the probability of phase transition to chaos tends to increase with network size, topological complexity and heterogeneity.[72–77] In particular, insertion of long-distance shortcuts according to small-world topology leads to chaos even in networks that cannot otherwise be chaotic.[78–81]

At the same time, *in-vitro* recordings of neuronal cultures on substrate-integrated multi-electrode arrays, indexing mesoscale activity in networks of $\approx 10^4$–10^5 neurons, demonstrate the emergence of self-organized small-world functional connectivity during culture maturation. It has separately been shown that the prevalence of chaotic activity in these cultures gradually increases as the number of active sites grows, in turn suggesting that the gradual formation of a dense and complex network promotes the emergence of chaos.[82,83]

E. Potential clinical relevance and study limitations

Elucidating the relationship between connectivity, spectral and non-linear dynamical features in the brain is potentially relevant to early diagnosis of Alzheimer's disease. It is an increasingly common neurodegenerative dementia, preferentially targeting the cortical hubs through heightened accumulation of toxic protein isoforms following intense synaptic metabolism.[84] While functional connectivity is significantly reduced in the precuneus and lateral parietal regions already in pre-symptomatic phases, the detectable alterations are inadequate for individual-case diagnosis; however, loss of synchronization may be accompanied or even preceded by changes in spectral and dynamical features, deeper understanding of which could be of substantial diagnostic benefit.[23,24,85] A recent finding of reduced amplitude of low-frequency fluctuations in the precuneus gradually tracking disease progression (connectivity loss) from cognitive normality to dementia is remarkably in agreement with the relationship between long-distance link strength and spectral shift observed here across regions of the healthy brain and for the networked chaotic oscillators.[86]

The present study has limitations that need consideration. First, while an empirical topographical correlation between functional connectivity and non-linearity was established, structural connectivity of the brain was not explicitly considered. Future work will need to address the question of whether functional connectivity, or structural connectivity as measurable using techniques diffusion-spectrum imaging, is more closely associated to heterogeneity of spectral content and non-linearity. The impact of node degree versus topological centrality also deserves further investigation. While in this work geodesic mapping was not performed, node degree of short- and long-range connectivity is significantly coupled across cortical regions; this incidentally also allays concerns over the impact of short-range correlation introduced by spatial Gaussian smoothing of the time-series.[87]

Second, only one spatiotemporal window (the one accessible to functional MRI) was considered, and it is necessary to determine whether the observed relationship also holds at finer temporal resolution (1 ms vs. 1 s scale) and on the microscopic and mesoscopic levels. This will help clarify if the observed relationships are generalizable rather than "epiphenomena" of specific experimental settings.

Third, the combined effects of non-stationarity, noise, geometric filtering, undersampling, and limited BOLD time-series length require deeper investigation, e.g., by means of synthetic data. While the temporal resolution (0.7 s) was higher than the majority of current resting-state functional MRI studies, it remains orders of magnitude away from the temporal scale of the underlying processes, and the results should be confirmed using emerging functional MRI datasets that have even higher temporal resolution (0.1 s) and correspondingly longer time-series length (>4000 points).[88]

VII. CONCLUSIONS

This paper has reported a topographical relationship across cortical areas of the healthy human brain between the node degree of functional connectivity, relative intensity of low-frequency activity, and evidence of non-linearity. High node degree was strongly associated with shift towards low-frequency activity (<0.1 Hz) and, although less markedly, also with evidence of non-linear structure, in the form of clearer saturation to a lower correlation dimension compared to Fourier amplitude and value distribution-adjusted surrogate data. Despite profound differences in scale, connectivity complexity, dynamics, and coupling mechanism, analogous effects were observed in a network of diffusively coupled single-transistor oscillators: at criticality, increased connectivity for nodes wired as extended hubs locally lead to chaos and associated large low-frequency cycle amplitude fluctuations. In accord with recent numerical results, we conjecture that a similar phenomenon could take place also in the brain. The observed homology between brain and single-transistor oscillator findings in our view motivates further investigation to better delineate the validity of networked chaotic oscillators as potential physical models of brain dynamics in health and disease.

ACKNOWLEDGMENTS

L.M. receives employment funding from Fondazione IRCCS Istituto Neurologico Carlo Besta (Milano, Italy) and Scienze Mente-Cervello (Rovereto, Italy). Brain data were provided by the Human Connectome Project, WU-Minn Consortium (Principal Investigators: David Van Essen and Kamil Ugurbil; 1U54MH091657) funded by the 16 NIH Institutes and Centers that support the NIH Blueprint for Neuroscience Research, and by the McDonnell Center for Systems Neuroscience at Washington University. The research of which the present work forms part is a collaborative project between the Fondazione IRCCS Istituto Neurologico Carlo Besta and the University of Trento, approved by the ethics committee of the former with decree No. 04 dated January 15, 2014. Experimental activities on chaotic oscillators were conducted at the University of Trento, funded partly by the same and partly by L.M. personally. L.M. is grateful to U. Hasson for interesting discussion in this area and to S. Tessari and B. Schmitz for technical assistance. The authors would also like to thank two anonymous reviewers for insightful feedback on an earlier version of this study.

[1] M. P. van den Heuvel and O. Sporns, J. Neurosci. **31**, 15775 (2011).
[2] O. Sporns, Ann. N.Y. Acad Sci. **1224**, 109 (2011).
[3] E. Bullmore and O. Sporns, Nat. Rev. Neurosci. **13**, 336 (2012).
[4] O. Sporns, Curr. Opin. Neurobiol. **23**, 162–171 (2013).
[5] D. R. Chialvo, Nat. Phys. **6**, 744 (2010).
[6] E. Tagliazucchi and D. R. Chialvo, AIP Conf. Proc. **1510**, 4 (2013).
[7] J. Cabral, M. L. Kringelbach, and G. Deco, Prog. Neurobiol. **114**, 102 (2014).
[8] J. Cabral, E. Hugues, O. Sporns, and G. Deco, Neuroimage **57**, 130 (2011).
[9] A. Haimovici, E. Tagliazucchi, P. Balenzuela, and D. R. Chialvo, Phys. Rev. Lett. **110**, 178101 (2013)
[10] S. Yu, H. Yang, O. Shriki, and D. Plenz, Front. Syst. Neurosci. **7**, 42 (2013).
[11] M. D. Fox and M. E. Raichle, Nat. Rev. Neurosci. **8**, 700 (2007).
[12] M. E. Raichle, Trends Cogn. Sci. **14**, 180 (2010).
[13] R. L. Buckner, J. Sepulcre, T. Talukdar, F. M. Krienen, H. Liu, T. Hedden, J. R. Andrews-Hanna, R. A. Sperling, and K. A. Johnson, J. Neurosci. **29**, 1860 (2009).
[14] M. P. van den Heuvel, R. C. Mandl, R. S. Kahn, and H. E. Hulshoff Pol, Hum. Brain Mapp. **30**, 3127 (2009).
[15] D. Tomasi and N. D. Volkow, Neuroimage **57**, 908 (2011).
[16] L. Minati, A. Nigri, M. Cercignani, and D. Chan, Med. Eng. Phys. **35**, 1525 (2013).
[17] N. K. Logothetis, Nature **453**, 869 (2008).
[18] J. C. Brooks, O. K. Faull, K. T. Pattinson, and M. Jenkinson, Front. Hum. Neurosci. **7**, 623 (2013).
[19] B. J. He, Trends Cogn. Sci. **18**, 480 (2014).
[20] M. Rubinov and E. Bullmore, Trends Cogn. Sci. **17**, 641 (2013).
[21] E. Tagliazucchi, P. Balenzuela, D. Fraiman, and D. R. Chialvo, Front. Physiol. **3**, 15 (2012).
[22] R. M. Hutchison, T. Womelsdorf, E. A. Allen, P. A. Bandettini, V. D. Calhoun, M. Corbetta, S. Della Penna, J. H. Duyn, G. H. Glover, J. Gonzalez-Castillo, D. A. Handwerker, S. Keilholz, V. Kiviniemi, D. A. Leopold, F. de Pasquale, O. Sporns, M. Walter, and C. Chang, Neuroimage **80**, 360 (2013).
[23] C. J. Stam, Clin. Neurophysiol. **116**, 2266 (2005).
[24] T. Takahashi, Prog. Neuropsychopharmacol. Biol. Psychiatry **45**, 258 (2013).
[25] L. D. Landau and E. M. Lifshitz, *Statistical Physics Part 1* (Butterworth-Heinemann, Oxford, 2003).
[26] E. Ott, *Chaos in Dynamical Systems* (Cambridge University Press, Cambridge, 2002).
[27] R. Hilborn, *Chaos and Nonlinear Dynamics: An Introduction for Scientists and Engineers Paperback* (Oxford University Press, Oxford, 2001).
[28] Q. H. Zou, C. Z. Zhu, Y. Yang, X. N. Zuo, X. Y. Long, Q. Cao, Y. F. Wang, and Y. F. Zang, J. Neurosci. Methods **172**, 137 (2008).
[29] K. Kalcher, R. N. Boubela, W. Huf, L. Bartova, C. Kronnerwetter, B. Derntl, L. Pezawas, P. Filzmoser, C. Nasel, and E. Moser, PLoS One **9**, e93375 (2014).
[30] G. Deco and V. K. Jirsa, J. Neurosci. **32**, 3366 (2012).
[31] L. Minati, Chaos **24**, 033110 (2014).
[32] L. Minati, Chaos **24**, 043108 (2014).
[33] K. Uğurbil, J. Xu, E. J. Auerbach, S. Moeller, A. T. Vu, J. M. Duarte-Carvajalino, C. Lenglet, X. Wu, S. Schmitter, P. F. Van de Moortele, J. Strupp, G. Sapiro, F. De Martino, D. Wang, N. Harel, M. Garwood, L. Chen, D. A. Feinberg, S. M. Smith, K. L. Miller, S. N. Sotiropoulos, S. Jbabdi, J. L. Andersson, T. E. Behrens, M. F. Glasser, D. C. Van Essen, and E. Yacoub, Neuroimage **80**, 80 (2013).
[34] S. M. Smith, C. F. Beckmann, J. Andersson, E. J. Auerbach, J. Bijsterbosch, G. Douaud, E. Duff, D. A. Feinberg, L. Griffanti, M. P. Harms, M. Kelly, T. Laumann, K. L. Miller, S. Moeller, S. Petersen, J. Power, G. Salimi-Khorshidi, A. Z. Snyder, A. T. Vu, M. W. Woolrich, J. Xu, E. Yacoub, K. Uğurbil, D. C. Van Essen, and M. F. Glasser, Neuroimage **80**, 144 (2013).
[35] M. F. Glasser, S. N. Sotiropoulos, J. A. Wilson, T. S. Coalson, B. Fischl, J. L. Andersson, J. Xu, S. Jbabdi, M. Webster, J. R. Polimeni, D. C. Van Essen, and M. Jenkinson, Neuroimage **80**, 105 (2013).
[36] See www.fil.ion.ucl.ac.uk/spm/software/spm8 for SPM8 software and related publications.
[37] L. Minati, D. Zacà, L. D'Incerti, and J. Jovicich, Med. Eng. Phys. **36**, 1212 (2014).
[38] H. Kantz and T. Schreiber, *Nonlinear Time Series Analysis* (Cambridge University Press, Cambridge, 1997).
[39] R. Hegger, B. Kantz, and T. Schreiber, Chaos **9**, 413 (1999).
[40] See www.mpipks-dresden.mpg.de/~tisean for TISEAN software and related publications.

[41] J. Theiler and S. Eubank, Chaos **3**, 771 (1993).
[42] P. Grassberger, R. Hegger, H. Kantz, C. Schaffrath, and T. Schreiber, Chaos **3**, 127 (1993).
[43] H. Kantz, T. Schreiber, I. Hoffmann, T. Buzug, G. Pfister, L. G. Flepp, J. Simonet, R. Badii, and E. Brun, Phys. Rev. E **48**, 1529 (1993).
[44] T. Schreiber and A. Schmitz, Phys. Rev. Lett. **77**, 635 (1996).
[45] F. Takens, *Dynamical Systems and Bifurcations*, Lecture Notes in Mathematics, Vol. 1125 (Springer, New York, 1985), pp. 99–106.
[46] M. Fraser and H. L. Swinney, Phys. Rev. A **33**, 1134 (1986).
[47] M. B. Kennel, R. Brown, and H. D. I. Abarbanel, Phys. Rev. A **45**, 3403 (1992).
[48] J. Theiler, J. Opt. Soc. Am. A **7**, 1055 (1990).
[49] A. Provenzale, L. A. Smith, R. Vio, and G. Murante, Physica D **58**, 31 (1992).
[50] P. Grassberger and I. Procaccia, Physica D **9**, 189 (1983).
[51] T. Schreiber, Phys. Rev. Lett. **78**, 843 (1997).
[52] J. K. Mai, G. Paxinos, and T. Voss, *Atlas of the Human Brain* (Academic Press, Waltham, MA, USA, 2007).
[53] A. E. Cavanna and M. R. Trimble, Brain **129**, 564 (2006).
[54] H. Peng, F. Long, and C. Ding, IEEE Trans. Pattern Anal. Mach. Intell. **27**, 1226 (2005).
[55] N. X. Vinh and J. Epps, J. Mach. Learn. Res. **11**, 2837 (2010).
[56] M. E. J. Newman, Phys. Rev. E **70**, 056131 (2004).
[57] See supplementary material at http://dx.doi.org/10.1063/1.4914938 for additional statistics table.
[58] G. Deco, V. K. Jirsa, and A. R. McIntosh, Nat. Rev. Neurosci. **12**, 43 (2011).
[59] Q. Zou, C. W. Wu, E. A. Stein, Y. Zang, and Y. Yang, Neuroimage **48**, 515 (2009).
[60] X. Di, E. H. Kim, C. C. Huang, S. J. Tsai, C. P. Lin, and B. B. Biswal, Front. Hum. Neurosci. **7**, 118 (2013).
[61] C. Triantafyllou, J. R. Polimeni, and L. L. Wald, Neuroimage **55**, 597 (2011).
[62] M. Smal, D. Yu, J. Simonotto, R. G. Harrison, N. Grubb, and K. A. A. Fox, Chaos Solitons Fractals **13**, 1755 (2002).
[63] M. P. Hanias and G. S. Tombras, Chaos Solitons Fractals **40**, 246 (2009).
[64] T. Gautama, D. P. Mandic, and M. M. Van Hulle, IEEE Trans. Med. Imaging **22**, 636 (2003).
[65] X. Xie, Z. Cao, and X. Weng, Neuroimage **40**, 1672 (2008).
[66] G. Deco, V. Jirsa, A. R. McIntosh, O. Sporns, and R. Kötter, Proc. Natl. Acad. Sci. U.S.A. **106**, 10302 (2009).
[67] A. Rădulescu and L. R. Mujica-Parodi, Neuroimage **90**, 436 (2014).
[68] S. Boccaletti, J. Kurths, G. Osipov, D. L. Valladares, and C. S. Zhou, Phys. Rep. **366**, 1 (2002).
[69] B. J. MacLennan, Int. J. Gen. Syst. **43**, 682 (2014).
[70] S. Boccaletti, V. Latora, Y. Moreno, M. Chavez, and D.-U. Hwang, Phys. Rep. **424**, 175 (2006).
[71] A. Arenas, A. Díaz-Guilera, J. Kurths, Y. Moreno, and C. Zhoug, Phys. Rep. **469**, 93 (2008).
[72] N. Bertschinger and T. Natschläger, Neural Comput. **16**, 1413 (2004).
[73] A. Zumdieck, M. Timme, T. Geisel, and F. Wolf, Phys. Rev. Lett. **93**, 244103 (2004).
[74] H. F. Zhang, R. X. Wu, and X. C. Fu, Chaos Solitons Fractals **28**, 472 (2006).
[75] T.-W. Ko and G. B. Ermentrout, Phys. Rev. E **78**, 026210 (2008).
[76] J. C. Sprott, Chaos **18**, 023135 (2008).
[77] L. Büsing, B. Schrauwen, and R. Legenstein, Neural Comput. **22**, 1272 (2010).
[78] H. Yang, F. Zhaob, and B. Wang, Physica A **364**, 544 (2006).
[79] H. Riecke, A. Roxin, S. Madruga, and S. A. Solla, Chaos **17**, 026110 (2007).
[80] W. J. Yuan, X. S. Luo, P. Q. Jiang, B. H. Wang, and J. Q. Fang, Chaos Solitons Fractals **37**, 799 (2008).
[81] R. Tönjes, N. Masuda, and H. Kori, Chaos **20**, 033108 (2010).
[82] W. Chen, X. Li, J. Pu, and Q. Luo, Phys. Rev. E **81**, 061903 (2010).
[83] J. H. Downes, M. W. Hammond, D. Xydas, M. C. Spencer, V. M. Becerra, K. Warwick, B. J. Whalley, and S. J. Nasuto, PLoS Comput. Biol. **8**, e1002522 (2012).
[84] W. de Haan, K. Mott, E. C. van Straaten, P. Scheltens, and C. J. Stam, PLoS Comput. Biol. **8**, e1002582 (2012).
[85] C. Y. Wee, P. T. Yap, K. Denny, J. N. Browndyke, G. G. Potter, K. A. Welsh-Bohmer, L. Wang, and D. Shen, PLoS One **7**, e37828 (2012).
[86] P. Liang, J. Xiang, H. Liang, Z. Qi, and K. Li, Curr. Alzheimer Res. **11**, 389 (2014).
[87] J. Sepulcre, H. Liu, T. Talukdar, I. Martincorena, B. T. Yeo, and R. L. Buckner, PLoS Comput. Biol. **6**, e1000808 (2010).
[88] H. L. Lee, B. Zahneisen, T. Hugger, P. LeVan, and J. Hennig, Neuroimage **65**, 216 (2013).